Title	In-structure shock of underground structures : a revisit with experimental investigation
Author(s)	Zhou, Hongyuan; Beppu, Masuhiro; Ma, Guowei; Zhao, Zhiye
Citation	Zhou, H., Beppu, M., Ma, G., & Zhao, Z. (2013). In-structure shock of underground structures: A revisit with experimental investigation. Engineering Structures, 56, 1620–1630.
Date	2013
URL	http://hdl.handle.net/10220/19376
Rights	© 2013 Elsevier Ltd. This is the author created version of a work that has been peer reviewed and accepted for publication by Engineering Structures, Elsevier Ltd.. It incorporates referee's comments but changes resulting from the publishing process, such as copyediting, structural formatting, may not be reflected in this document. The published version is available at: [http://dx.doi.org.ezlibproxy1.ntu.edu.sg/10.1016/j.engstruct.2013.07.037].

In-structure shock of underground structures: a revisit with experimental investigation

(*Engineering Structures*, Vol. 56, 1620-1630, November 2013)

Hongyuan Zhou[a], Masuhiro Beppu[b], Guowei Ma[c]*, Zhiye Zhao[d]

[a,d] *School of Civil and Environmental Engineering, Nanyang Technological University, Singapore 639798, Singapore*

[b] *Department of Civil and Environmental Engineering, National Defense Academy, Yokosuka, Kanagawa, 239-8686, Japan*

[c] *School of Civil and Resources Engineering, the University of Western Australia, WA 6009, Australia*

* Corresponding author: Guowei Ma

Professor

School of Civil and Resource Engineering

the University of Western Australia

35 Stirling Highway, Crawley WA6009

Australia

Tel: 61-8-6488-3102

Fax: 61-8-6488-1018

E-mail address: ma@civil.uwa.edu.au (G.W. Ma).

Abstract: In-structure shock of underground structures subjected to ground shocks is investigated, both theoretically and experimentally. In the theoretical prediction, the ground shock is simplified to a triangular pulse with a rise time. It is found that the acceleration time history of the structure when the rise time of the ground shock is considered is significantly different from that when it is neglected. A small scale test is designed and conducted to validate the theoretical prediction. The comparison of the measured and predicted acceleration time histories suggests that the theoretical prediction with ground shock rise time considered is more reasonable. Further, shock response spectra for the equipment attached to the underground structure are established and a case study indicates that in-structure shock level of the devices predicted by the model with ground shock rise time is higher than that predicted without consideration of the ground shock rise time. It is shown that the present assessment of in-structure shock is reasonably accurate and it can be used for a preliminary design of underground structures where in-structure shock is concerned.

Keywords: In-structure shock, Ground shock, Blast load, Underground structure, Shock response spectra, Experiment.

Notation

A	Cross-sectional area of beam
c_s	Acoustic velocity of soil
E	Young's modulus of concrete
f	Coupling factor of explosion energy to soil
h	Thickness of beam
I	Moment of inertia of beam cross-section
l	Length of beam
m	Attenuation coefficient of stress wave in soil
p	Linear intensity of uniform load on beam
P_0	Free-field peak pressure
R	Distance between explosion center and buried structure
t	Time starting at arrival of ground shock
w	Deflection of beam
W	TNT equivalent charge weight
α	Reduction factor
β	A factor equal to 160 in imperial unit system
ε	Strain at beam mid-span
v	Poisson's ratio of concrete
ρ	Mass density of concrete
ρ_s	Mass density of soil
ω_n	nth mode circular natural frequency
ζ_n	nth mode interfacial damping ratio
$\sigma_f(t)$	Free field pressure time history of ground shock
σ_m	Maximum stress
σ_y	Yield strength of mild steel
λ	Ratio of rise time to ground shock duration

1. Introduction

Some protective structures are embedded in soil to provide a safer environment for the containment of personnel and equipment. Nevertheless, the environment within underground structures in recent years is not as safe as decades ago; with the development of penetration weapons, the depth of the subsurface detonations can be extremely large and the explosions can be possible in any location around, even beneath, an underground structure. In addition to the situations where the underground structure is totally destroyed by a close-range subsurface detonation, if the standoff distance, the distance between the explosion center and the buried structure, is neither too long nor too short, the soil-transmitted blast, or ground shock, may cause critical vibrations and damage the contained equipment, while little or no damage of the underground structure occurs. This kind of severe vibration, not damaging the main structure, but damaging contained devices, is termed as in-structure shock [1]. Besides research on damage and protection measures of buried structures in terms of strength [2-7], the study on in-structure shock of underground structures is equally important [8-14] since failure in any aspect, either strength or serviceability, completely prevents the structure from accomplishing its designed tasks.

Equipment and devices, with increasing complexity, become increasingly vulnerable to excessively high accelerations induced by strong vibrations. While smooth operation of complicated devices is vital in ensuing functions of underground structures, prior to a detailed design, construction and possible shock isolation, the vibration environment within the structure should be carefully examined and judiciously defined.

In assessing in-structure shock of underground structures subjected to subsurface blasts,

the dynamic soil-structure interaction was considered and the responses of structural members were studied [11, 15, 16]. The ground shock in these models, is characterized as a short-duration triangular load with zero rise time, which is believed to be a reasonable idealization of the real shock load.

In major design provisions, e.g., TM5-855-1, the free field peak pressure and duration of a ground shock are estimated empirically with known soil parameters, equivalent TNT charge weight, and standoff distance. Besides, the rise time of a ground shock is assumed 1/10 of the arrival time. Recall the blast duration is twice that of the arrival time [12, 16], the assumed rise time is thus equal to 1/20 of the blast duration. In fact, while the intensity of a ground shock attenuates with distance traveled, its duration elongates and the ratio of rise time to total duration increases [17-18].

When a typical underground structure subjected to a ground shock is analyzed where the maximum deflection of a specific structural member is of most concern, the influence of the rise time can be neglected since no matter whether the rise time is accounted for or not, the specific impulses (impulse per unit area) remain the same, and the impulse dominates the structural behavior provided that the ground shock duration is significantly shorter than the primary natural period of the concerned structural member [19-21], which is always true in engineering practice.

When it comes to in-structure shock of underground structures, however, things are different. As second derivative of displacement time history with respect to time, acceleration time history depends on the displacement time history, rather than the maximum deflection. Therefore to predict the in-structure shock effect on the contained devices, the detailed

excitation time history (in fact the acceleration time history of underground structural member to which the equipment is attached) rather than the peak value, is required. To date, the effect of ground shock rise time on in-structure shock of underground structures has not been examined. Take the structural response at time zero to analyze, with a zero rise time, the initial acceleration of the structural member of concern is non-zero; and with a non-zero rise time, the initial acceleration of the member is zero. The acceleration time histories of the structural member in the two abovementioned cases, in fact the excitation for the secondary structures within the main structure [22], may be substantially different and result in significantly different in-structure shock level on the contained equipment.

One major consideration of assuming zero rise time of ground shocks in analysis is that the acceleration time history with a high initial peak is believed to be severer than that from a similar ground shock with non-zero rise time, leading to a stronger shock level imposed on the inside equipment, based on which the design is conservative. This seemingly reasonable consideration, however, is not necessarily correct since the shock level on the inside equipment depends on not only the excitation, but also the properties of equipment itself. Therefore, it is meaningful and necessary to re-examine in-structure shock of underground structures subjected to ground shocks with non-zero rise time.

In the present study, theoretical prediction of the structural member response of an underground structure subjected to a ground shock is derived, with a non-zero rise time taken into consideration. The structural response is assumed elastic due to the relative large standoff distance, where in-structure shock is the major concern. Then a small scale test is designed and conducted to validate the theoretical prediction. With the test parameters, a case study

with theoretical prediction in the present study is carried out and compared with the test data. Finally, a discussion is presented on influence of the ground shock rise time on in-structure shock of underground structures, followed by recommendations for shock level assessment in engineering practice.

The greatest threat to the equipment and the underground structure is detonations from beneath the floor. The present study intends to simulate this serious scenario: the explosion is beneath the structure and loads the floor. In fact, there is no difference in nature between a beneath blast loading the floor and a side burst loading the walls. For convenience, in the test, horizontal set-up is used to simulate the scenario where the detonation is from beneath the structure and loads the floor.

2. Response of a structural member of a buried structure subjected to a ground shock with non-zero rise time

A typical underground structure is subjected to a ground shock induced by a subsurface detonation, shown in Fig. 1. Among the possible detonation positions, location 1 is most critical with the same standoff distance since generally the devices and personnel are on the floor, thus analyzed in the present study. The purpose of the current study is to demonstrate a general approach to predict the in-structure shock of underground structures, with an emphasis on the effect of ground shock rise time on in-structure shock. Material is not specified in the model, therefore the model can be used for structures of various materials, for instance, reinforced concrete which is frequently used in constructing subsurface facilities.

With the rise time taken into consideration, the ground shock is simplified as a triangular load with a relatively sharp rise, illustrated in Fig. 2. The simplified free-field load is in a piecewise form:

$$\sigma_f(t)=\begin{cases}\dfrac{P_0\alpha t}{\lambda T_d} & for\ t\le\lambda T_d\\ \dfrac{P_0\alpha\left(T_d-t\right)}{\left(1-\lambda\right)T_d} & for\ \lambda T_d<t\le T_d\end{cases} \tag{1}$$

the peak pressure [1]:

$$P_0=\beta f\left(\rho_s c_s\right)\left(\frac{R}{W^{1/3}}\right)^{-m} \tag{2}$$

where $\sigma_f(t)$ is the free field ground shock time history; P_0 is the free-field peak pressure, in psi; f is a dimensionless coupling factor of the explosion energy to soil; α is a reduction factor, defined as ratio of the equivalent uniform pressure on a wall or floor of the structure to the maximum pressure of the actual load distribution; $\rho_s c_s$ is the acoustic impedance of soil, in psi/fps; m is an attenuation coefficient, dimensionless; W is the TNT equivalent charge weight, in lb; R is the distance measured from the explosion center to the structure, in ft; β is a factor equal to 160 in the imperial unit system, dimensionless; and λ is dimensionless, representing the ratio of rise time to blast duration. It should be noted that the pressure calculated in psi is converted to SI unit system in Pa before being used in further calculation.

For a typical underground structure subjected to a typical subsurface detonation, it is the initial stage of acceleration time history that majorly contributes to the shock on the equipment while the other part only has negligible contribution [12]. Therefore in the present study, response of the structural member within the blast duration is sufficient and the post-blast phase is neglected. In addition, the influence of the global rigid body motion of the

entire structure on the member response is insignificant [13] and thus not considered.

In engineering practice, a structural member with one dimension greater than twice the other or only supported at the opposite edges, namely one-way slab, is often simplified and analyzed with a modified plane strain beam model [12]. The boundary of the idealized beam representing the structural member is neither fixed nor simply supported. In the present study, simply supported boundary condition is used to yield a conservative prediction. Besides, in the small-scale test, a square structural member with two opposite edges constrained and other two edges free, can be idealized as a modified beam to analyze. Further, in the analysis of an underground structure where the in-structure shock is the major concern, generally the standoff distance from the explosion center to the structure is relatively distant. As a result, the curvature of the free-field ground shock induced by a typical spherical buried charge can be neglected and the load on the structural member is simplified as a plane wave.

The response of a structural member subjected to a ground shock with non-zero rise time, with dynamic soil-structure interaction considered, is derived. The governing equation of a beam under dynamic load is:

$$EI\frac{\partial^4 w(x,t)}{\partial x^4}+\rho A\frac{\partial^2 w(x,t)}{\partial t^2}=P(x,t) \tag{3}$$

Recall the dynamic soil-structure interaction [11-16], the equation can be re-written as:

$$EI\frac{\partial^4 w(x,t)}{\partial x^4}+\rho A\frac{\partial^2 w(x,t)}{\partial t^2}=2\sigma_f(t)-\rho_s c_s\frac{\partial w(x,t)}{\partial t} \tag{4}$$

For convenience, the triangular free-field load is divided into two parts, the increasing part and the decreasing part.

2.1 Phase I: 0<t< λT_d

In the phase when the load increase linearly, the governing equation is:

$$EI\frac{\partial^4 w(x,t)}{\partial x^4}+\rho A\frac{\partial^2 w(x,t)}{\partial t^2}+\rho_s c_s\frac{\partial w(x,t)}{\partial t}=2\frac{P_0\alpha}{\lambda T_d}t \tag{5}$$

The initial condition is zero displacement and velocity. Assume the displacement as:

$$w(x,t)=\sum_{n=1}^{\infty}W_n(x)q_n(t) \tag{6}$$

where $W_n(x)$ is the *n*th mode shape and $q_n(t)$ is the *n*th general coordinate.

The solution consists of infinite terms and the displacement corresponding to the nth mode is: $w_n(x,t)=W_n(x)q_n(t)$. The *n*th mode natural frequency:

$$\omega_n=\sqrt{\frac{EI}{\rho A}}\left(\frac{n\pi}{l}\right)^2,\quad W_n(x)=\sqrt{\frac{2}{\rho Al}}\sin\frac{n\pi x}{l} \tag{7}$$

Combination of Eq. (5) and Eq.(6) yields:

$$\rho A\sum_{n=1}^{\infty}\omega_n^2 W_n(x)q_n(t)+\rho_s\sum_{n=1}^{\infty}W_n(x)\dot{q}_n(t)c_s=2\frac{P_0\alpha}{\lambda T_d}t \tag{8}$$

According to the orthogonality of the modes, the governing equation in the generalized space:

$$\ddot{q}_n(t)+\frac{\rho_s c_s}{\rho A}\dot{q}_n(t)+\omega_n^2 q_n(t)=2\left[1-(-1)^n\right]\frac{l}{n\pi}\sqrt{\frac{2}{\rho Al}}\frac{P_0\alpha}{\lambda T_d}t \tag{9}$$

define

$$\zeta_n=\frac{\frac{\rho_s c_s}{\rho A}}{2\omega_n} \tag{10}$$

Equation (9) is re-written as:

$$\ddot{q}_n(t)+2\zeta_n\omega_n\dot{q}_n(t)+\omega_n^2 q_n(t)=2\left[1-(-1)^n\right]\frac{l}{n\pi}\sqrt{\frac{2}{\rho Al}}\frac{P_0\alpha}{\lambda T_d}t \tag{11}$$

Until now, with the governing equation and initial conditions, the structural responses

can be determined. The interfacial damping, defined in Eq. (10), delineates how the soil interacts with and affects the structural response. Generally, the system consisting of the structural member and the surrounding soil may have three damping ratios, over-damping, under-damping and critical damping, under which the structural responses are as follows:

Overly-damped: $\zeta_n = \dfrac{\dfrac{\rho_s c_s}{\rho A}}{2\omega_n} > 1$

The displacement contribution of *n*th mode in generalized space is:

$$q_n(t) = E_n e^{D_{n,1} t} + F_n e^{D_{n,3} t} + \frac{2D_{n,1}}{\omega_n^2 \lambda T_d}\left(t - \frac{2\zeta_n}{\omega_n}\right) \tag{12}$$

where

$$E_n = -\frac{D_{n,1}\left(2\zeta D_{n,3} + \omega_n\right)}{\omega_n^4 \lambda T_d \sqrt{\zeta_n^2 - 1}}, \quad F_n = \frac{D_{n,1}\left(2\zeta D_{n,2} + \omega_n\right)}{\omega_n^4 \lambda T_d \sqrt{\zeta_n^2 - 1}}$$

$$D_{n,1} = \left[1 - (-1)^n\right]\frac{l}{n\pi}\sqrt{\frac{2}{\rho A l}} P_0, \quad D_{n,2} = \left(-\zeta_n + \sqrt{\zeta_n^2 - 1}\right)\omega_n, \quad D_{n,3} = \left(-\zeta_n - \sqrt{\zeta_n^2 - 1}\right)\omega_n$$

The velocity and the acceleration contributions are:

$$\dot{q}_n(t) = E_n D_{n,2} e^{D_{n,2} t} + F_n D_{n,3} e^{D_{n,3} t} + \frac{2D_{n,1}}{\omega_n^2 \lambda T_d} \tag{13}$$

$$\ddot{q}_n(t) = E_n D_{n,2}^2 e^{D_{n,2} t} + F_n D_{n,3}^2 e^{D_{n,3} t} \tag{14}$$

Under-damped: $\zeta_n = \dfrac{\dfrac{\rho_s c_s}{\rho A}}{2\omega_n} < 1$

The *n*th mode displacement time history in the generalized space is:

$$q_n(t) = e^{-\zeta_n \omega_n t}\left[E_n \sin\left(D_{n,4} t\right) + F_n \cos\left(D_{n,4} t\right)\right] + \frac{2D_{n,1}}{\omega_n^2 \lambda T_d}\left(t - \frac{2\zeta_n}{\omega_n}\right) \tag{15}$$

where

$$E_n = \frac{2\left(2\zeta_n^2 - 1\right)D_{n,1}}{\omega_n^2 \lambda T_d D_{n,4}}, \quad F_n = \frac{4\zeta_n D_{n,1}}{\omega_n^3 \lambda T_d}, \quad D_{n,4} = \sqrt{1-\zeta_n^2}\,\omega_n$$

The velocity and acceleration contributions are:

$$\dot{q}_n(t) = e^{-\zeta_n \omega_n t}\left[-\left(\zeta_n \omega_n E_n + D_{n,4} F_n\right)\sin\left(D_{n,4} t\right) + \left(D_{n,4} E_n - \zeta_n \omega_n F_n\right)\cos\left(D_{n,4} t\right)\right] + \frac{2D_{n,1}}{\omega_n^2 \lambda T_d} \tag{16}$$

$$\ddot{q}(t) = e^{-\zeta_n \omega_n t}\left\{\begin{array}{l}\left[\omega_n^2 E_n\left(2\zeta_n^2 - 1\right) + 2\omega_n \zeta_n F_n D_{n,4}\right]\sin\left(D_{n,4} t\right) \\ +\left[-2\omega_n \zeta_n D_{n,4} E_n + \omega_n^2 F_n\left(2\zeta_n^2 - 1\right)\right]\cos\left(D_{n,4} t\right)\end{array}\right\} \tag{17}$$

The situation of critical damping can be categorized as overly-damped due to the similar physical and mathematical nature. The displacement, velocity, and acceleration of the structural element should be the summation of contributions from different modes, i.e.,

$$w(x,t) = \sum_{n=1}^{\infty} W_n(x)\, q_n(t) \tag{18a}$$

$$\dot{w}(x,t) = \sum_{n=1}^{\infty} W_n(x)\, \dot{q}_n(t) \tag{18b}$$

$$\ddot{w}(x,t) = \sum_{n=1}^{\infty} W_n(x)\, \ddot{q}_n(t) \tag{18c}$$

2.2 Phase II: $\lambda T_d < t < T_d$

In fact, the initial condition of this phase is the terminal condition of the preceding phase. For convenience, offset the time axis by λT_d with the new time axis $t_1 = t - \lambda T_d$.

The decreasing load time history in the new time axis is:

$$\sigma_f(t_1) = P_0 \alpha\left[1 - \frac{t_1}{(1-\lambda)T_d}\right] \tag{19}$$

The governing equation is:

$$EI\frac{\partial^4 w(x,t_1)}{\partial x^4}+\rho A\frac{\partial^2 w(x,t_1)}{\partial t_1^2}+\rho_s c_s\frac{\partial w(x,t_1)}{\partial t_1}=2P_0\alpha\left[1-\frac{t_1}{(1-\lambda)T_d}\right] \tag{20}$$

and the initial conditions in this phase:

$$G_n=q_n(t=\lambda T_d),\quad H_n=\dot{q}_n(t=\lambda T_d) \tag{21}$$

Introducing the interfacial damping, the governing equation in the generalized space is:

$$\ddot{q}_n(t_1)+2\zeta_n\omega_n\dot{q}_n(t_1)+\omega^2 q_n(t_n)=2\left[1+(-1)^n\right]\frac{l}{n\pi}\sqrt{\frac{2}{\rho Al}}P_0\alpha\left[1-\frac{t_1}{(1-\lambda)T_d}\right] \tag{22}$$

Similarly, the responses of the structural member are:

Overly-damped: $\zeta_n=\dfrac{\dfrac{\rho_s c_s}{\rho A}}{2\omega_n}>1$

The *n*th mode displacement contribution in the generalized space is:

$$q_n(t_1)=E_n e^{D_{n,1}t_1}+F_n e^{D_{n,2}t_1}+2\frac{D_{n,1}}{\omega_n^2}\left[1-\frac{t_1}{(1-\lambda)T_d}+\frac{2\zeta_n}{(1-\lambda)\omega_n T_d}\right] \tag{23}$$

where

$$E_n=\frac{1}{2\omega_n\sqrt{\zeta_n^2-1}}\left\{H_n+\frac{2D_{n,1}}{(1-\lambda)\omega_n^2 T_d}-D_{n,3}\left\{G_n-2\frac{D_{n,1}}{\omega_n^2}\left[1+\frac{2\zeta_n}{(1-\lambda)\omega_n T_d}\right]\right\}\right\}$$

$$F_n=-\frac{1}{2\omega_n\sqrt{\zeta_n^2-1}}\left\{H_n+\frac{2D_{n,1}}{(1-\lambda)\omega_n^2 T_d}-D_{n,2}\left\{G_n-2\frac{D_{n,1}}{\omega_n^2}\left[1+\frac{2\zeta_n}{(1-\lambda)\omega_n T_d}\right]\right\}\right\}$$

The velocity and acceleration contributions are:

$$\dot{q}_n(t_1)=E_n D_{n,2}e^{D_{n,2}t_1}+F_n D_{n,3}e^{D_{n,3}t_1}-\frac{2D_{n,1}}{(1-\lambda)\omega_n^2 T_d} \tag{24}$$

$$\ddot{q}_n(t_1)=E_n D_{n,2}^2 e^{D_{n,1}t_1}+F_n D_{n,3}^2 e^{D_{n,2}t_1} \tag{25}$$

Under-damped: $\zeta_n = \dfrac{\dfrac{\rho_s c_s}{\rho A}}{2\omega_n} < 1$

The *n*th mode displacement contribution in the generalize space is:

$$q_n(t_1) = e^{-\zeta_n \omega_n t_1}\left[E_n \sin\left(D_{n,4} t_1\right) + F_n \cos\left(D_{n,4} t_1\right)\right] + 2\frac{D_{n,1}}{\omega_n^2}\left[1 - \frac{t_1}{(1-\lambda)T_d} + \frac{2\zeta_n}{(1-\lambda)\omega_n T_d}\right] \quad (26)$$

where

$$E_n = \frac{1}{D_{n,4}}\left\{H_n + \zeta_n \omega_n\left[G_n - 2\frac{D_{1,n}}{\omega_n^2}\left(1 + \frac{2\zeta_n}{(1-\lambda)\omega_n T_d}\right)\right] + 2\frac{D_{n,1}}{(1-\lambda)\omega_n^2 T_d}\right\}$$

$$F_n = G_n - 2\frac{D_{1,n}}{\omega_n^2}\left[1 + \frac{2\zeta_n}{(1-\lambda)\omega_n T_d}\right]$$

And the velocity and acceleration contributions are:

$$\dot{q}_n(t_1) = e^{-\zeta_n \omega_n t_1}\left[-\left(\zeta_n \omega_n E_n + D_{n,4} F_n\right)\sin\left(D_{n,4} t_1\right) + \left(D_{n,4} E_n - \zeta_n \omega_n F_n\right)\cos\left(D_{n,4} t_1\right)\right] - 2\frac{D_{n,1}}{(1-\lambda)\omega_n^2 T_d} \quad (27)$$

$$\ddot{q}(t_1) = e^{-\zeta_n \omega_n t_1}\left\{\begin{array}{l}\left[\omega_n^2 E_n\left(2\zeta_n^2 - 1\right) + 2\omega_n \zeta_n F_n D_{n,4}\right]\sin\left(D_{n,4} t_1\right) + \\ \left[-2\omega_n \zeta_n D_{n,4} E_n + \omega_n^2 F_n\left(2\zeta_n^2 - 1\right)\right]\cos\left(D_{n,4} t_1\right)\end{array}\right\} \quad (28)$$

The displacement, velocity and acceleration of the structural member in this phase:

$$w(x, t_1) = \sum_{n=1}^{\infty} W_n(x)\, q_n(t_1) \quad (29a)$$

$$\dot{w}(x, t_1) = \sum_{n=1}^{\infty} W_n(x)\, \dot{q}_n(t_1) \quad (29b)$$

$$\ddot{w}(x, t_1) = \sum_{n=1}^{\infty} W_n(x)\, \ddot{q}_n(t_1) \quad (29c)$$

It is worth noting that throughout the analysis, dynamic soil-structure interaction is incorporated by introducing an interfacial damping and it is assumed that there is no

separation between the structural member and the surrounding soil. In fact, there may be separation and re-contact between them. For a typical underground structure subjected to a ground shock, however, the difference between considering the separation or not is not significant [14]. In fact, from the acceleration time histories in the present study, only the initial parts of these histories mainly contribute to the in-structure shock.

3. Experiment set-up

Generally, underground facilities are installed in soil with small acoustic impedance and large attenuation coefficient such as sand and soft soil; otherwise, backfilling is necessary. In the present study, to realistically simulate the soil-transmitted blast, wet fine sand is used as surrounding soil. A large cylinder of diameter 4 m is filled with wet fine sand and the experimental set-up is installed in the middle part. Based on the characteristic dimension of the test site and the acoustic velocity of the wet fine sand, the reflections from the cylinder boundary have no influence on the response of the test structural member thus the test can be considered as being carried out in an infinite medium. The overall design of the experiment is illustrated in Fig. 3.

The nature of in-structure shock of underground facilities is equipment failure under the damaging excessive acceleration induced by soil-transmitted blast load, in which the main structure only experiences minor or even no damage. Therefore it is reasonable to analyze the elastic structural responses of the main structure. To ensure elastic deformation, a small scale test is judiciously designed where mild steel plate and marble block are used to represent an underground structure.

To simulate a box-typed underground structure, a test system of one mild steel plate with two channel beams as supports, clamps as well as the marble block are constructed. The mass of the front plate is significantly small compared to the total mass of the test system consisting of the plate, channel beams, wood blocks as well as the steel clamps and the marble block shown in Fig. 3. The structural element nearest to the subsurface detonation is represented by the steel plate. In engineering practice where an underground structure is constructed, the boundary condition for this structural member is attached to other four members: neither simply supported nor fixed. In fact, its constraint effect is in between. In the current test, this effect is realized by the clamps with wood blocks, shown in Fig. 4(a): the constraints are stronger than simply supported and weaker than fixed boundaries. For convenience of constructing the test set-up, the other two boundaries are kept free and the mild steel plate is analyzed with a modified beam model. When backfilling the test set-up with wet fine sand, another plate is used to cover the space between the steel plate and the marble block so that the sand above will not fall into the space. Then the ground shock loads the steel plate only from outside and it cannot get in behind plate, which is the same as in the real underground structures subjected to ground shock.

The equipment or devices attached to the main structure is not simulated in the present test since once the responses, especially the acceleration time history, of the structural member are obtained, the maximum acceleration experienced by the equipment can be readily obtained with the well established shock response spectrum method [22].

An accelerometer and strain gauges are connected to the plate center. First the test system is installed in wet fine sand then backfilled. In the present study, the ratio of rise time to blast

duration is adopted as 0.1. It is taken from the free field pressure time histories induced by subsurface detonations in exactly the same test condition [23]. The small-scale tests were conducted in National Defense Academy, Japan.

4. Determination of the standoff distance and plate dimensions

To ensure the steel plate representing the structural member to deform elastically, based on the parameters of soil, charge type and weight, the required relationship between the standoff distance and plate dimensions is determined as follows.

The design of the plate (simplified as a modified beam, due to the boundary condition of two opposite edges simply supported and other two edges free) should be conservative, to ensure the plate to remain elastic throughout the test. Otherwise, the plastic zone will absorb additional energy and lead to inaccurate in-structure shock prediction, which should be avoided.

The plate in the test is subjected to relatively distant ground shock induced by subsurface detonation, which can be idealized as uniformly distributed load with triangular time-varying magnitude.

The methodology of determining the span-to-thickness ratio is a combination of static and dynamic approach. First, the dynamic response factor (DRF) (time-varying), defined as the ratio of the dynamic response to the response with the peak load statically applied, is determined with the lump-mass idealization [19]. Then a conservative maximum DRF is applied to modify the static load applied on the plate. Subsequently, the span-to-thickness ratio is determined by the dynamically-modified static approach. The two-step procedure is:

4.1 Step I: Determine the maximum dynamic response factor

According to Biggs [19], the modified beam can be idealized into a lump-mass SDOF model consisting of a mass and massless spring. In the idealization, taking shape function as the deflection curve under corresponding static load yields satisfactory approximation [19]:

$$\phi(x)=\frac{16}{5}\left(\frac{x}{L}-\frac{2x^3}{L^3}+\frac{x^4}{L^4}\right),\ \ 0\le x\le L \qquad [24] \tag{30}$$

where L is the beam span and x is the distance from one support.

The response of the idealized lump-mass system subjected to the ground shock with non-zero rise time can be obtained by solving the governing equations with initial conditions for the three loading phases (ground shock rising phase, ground shock decreasing phase, and post-shock phase) respectively. It is worth noting that the initial conditions of the ground shock decreasing phase and post-shock phase in fact are the terminal conditions of the preceding phases, respectively.

Here, a quicker approach is adopted: the three-phase piecewise loading is considered as the superposition of three linear ramp loadings with infinite duration, all starting from zero but with different starting time, as shown in Fig. 5. Subsequently, the response of the system is the superposition of the responses induced by these three loadings. The superposition principle holds since the system is linear.

The idealized ground shock loading can be written as:

$$p(t)=\frac{P_0}{\lambda T_d}t-\frac{P_0}{\lambda(1-\lambda)T_d}(t-\lambda T_d)H(t-\lambda T_d)+\frac{P_0}{(1-\lambda)T_d}(t-T_d)H(t-T_d) \tag{31}$$

where $H(\bullet)$ is the Heaviside function with $H(x\text{-}a)=1$ for $x\ge a$ and $H(x\text{-}a)=0$ for $x<a$. In greater detail, the loading can be written as:

$$p(t)=\begin{cases}\dfrac{P_0}{\lambda T_d}t & 0\le t\le \lambda T_d \\ \dfrac{P_0}{\lambda T_d}t-\dfrac{P_0}{\lambda(1-\lambda)T_d}(t-\lambda T_d) & \lambda T_d\le t\le T_d \\ \dfrac{P_0}{\lambda T_d}t-\dfrac{P_0}{\lambda(1-\lambda)T_d}(t-\lambda T_d)+\dfrac{P_0}{(1-\lambda)T_d}(t-T_d) & T_d\le t\end{cases} \tag{32}$$

It is well established that the response of a linear SDOF system to ramp load is

$$u(t)=\frac{P_s}{k}\left(\frac{t}{t_s}-\frac{\sin\omega t}{\omega t_s}\right) \qquad [20] \tag{33}$$

where P_s is certain force and t_s is the time instant corresponding to the force, thus P_s/t_s defines the gradient of the ramp loading. Then with superposition method and recall the different starting times, the response of the system is:

$$u(t)=\begin{cases}\dfrac{P_0}{k}\left(\dfrac{t}{\lambda T_d}-\dfrac{\sin\omega t}{\omega\lambda T_d}\right) & 0\le t\le \lambda T_d \\ \dfrac{P_0}{k}\left[\dfrac{1}{1-\lambda}-\dfrac{t}{(1-\lambda)T_d}-\dfrac{\sin\omega t}{\omega\lambda T_d}+\dfrac{\sin\omega(t-\lambda T_d)}{\omega\lambda(1-\lambda)T_d}\right] & \lambda T_d\le t\le T_d \\ \dfrac{P_0}{k}\left[-\dfrac{\sin\omega t}{\omega\lambda T_d}+\dfrac{\sin\omega(t-\lambda T_d)}{\omega\lambda(1-\lambda)T_d}-\dfrac{\sin\omega(t-T_d)}{\omega(1-\lambda)T_d}\right] & T_d\le t\end{cases} \tag{34}$$

Recall the deflection of the concerned system subjected to the peak static load $u_{st}=P_0/k$ and relationship between the natural circular frequency and the natural period of the system $\omega=2\pi/T$, the dynamic response factor time history with respect to non-dimensional time (defined as the ratio of time to natural period of the SDOF system) is:

$$\frac{u(t)}{u_{st}}=\begin{cases}\dfrac{T}{\lambda T_d}\dfrac{t}{T}-\dfrac{\dfrac{T}{T_d}\sin 2\pi\dfrac{t}{T}}{2\pi\lambda} & 0\le\dfrac{t}{T_d}\le\lambda \quad or \quad 0\le\dfrac{t}{T}\le\lambda\dfrac{T_d}{T} \\ \dfrac{1}{1-\lambda}-\dfrac{T}{(1-\lambda)T_d}\dfrac{t}{T}-\dfrac{\dfrac{T}{T_d}\sin 2\pi\dfrac{t}{T}}{2\pi\lambda}+\dfrac{\dfrac{T}{T_d}\sin 2\pi\left(\dfrac{t}{T}-\lambda\dfrac{T_d}{T}\right)}{2\pi\lambda(1-\lambda)} & \lambda\le\dfrac{t}{T_d}\le 1 \quad or \quad \lambda\dfrac{T_d}{T}\le\dfrac{t}{T}\le\dfrac{T_d}{T} \\ -\dfrac{\dfrac{T}{T_d}\sin 2\pi\dfrac{t}{T}}{2\pi\lambda}+\dfrac{\dfrac{T}{T_d}\sin 2\pi\left(\dfrac{t}{T}-\lambda\dfrac{T_d}{T}\right)}{2\pi\lambda(1-\lambda)}-\dfrac{\dfrac{T}{T_d}\sin 2\pi\left(\dfrac{t}{T}-\dfrac{T_d}{T}\right)}{2\pi(1-\lambda)} & 1\le\dfrac{t}{T_d} \quad or \quad \dfrac{T_d}{T}\le\dfrac{t}{T}\end{cases} \tag{35}$$

If the rise time is remarkably shorter than the total ground shock duration, the load becomes triangular with zero rise time. Further, if the blast duration is significantly longer than the natural period of the system, the load becomes step constant load with infinite duration. From Eq. (35), the upper bound for the maximum dynamic response factor is 2.

Conservatively, the maximum factor is taken as 2 to ensure the plate to remain elastic throughout the test. For linear systems which allows superposition of load and response such as the present study, the span-to-thickness ratio of the plate can be determined by static approach with uniformly distributed load amplified by dynamic factor.

In the test, the deflection direction of the plate is perpendicular to the gravity, therefore the gravity effect on the plate deflection is trivial and can be neglected.

4.2 Determine the span-to-thickness ratio

For a beam subjected to a uniformly distributed load, the maximum bending moment at the mid-span is:

$$M_{max}=\frac{pl^2}{8} \tag{36}$$

where p is the linear intensity of the uniform load, l is the span of the beam.

When the beam is loaded, the design load applied is four times the free-field peak pressure. The factor 4 is from two aspects: the maximum dynamic response factor 2 and the factor for full reflection of ground shock 2.

$$p = 4P_0 \tag{37}$$

where P_0 is the peak value of the induced free-field pressure from the subsurface blast, as previously defined. On one hand, the actual maximum dynamic factor is less than 2; On the other hand, the factor for ground shock reflection is also less than 2. Only at the instant of shock arrival, the full reflection yield a factor of exactly 2. Therefore the equivalent static load is over-estimated and the design is conservative.

The maximum stress under uniform-load-caused-bending is:

$$\sigma_m = \frac{M_{\max}}{\frac{h^3}{12}} \frac{h}{2} \tag{38}$$

where h is the beam thickness. For convenience, the beam width is taken as unit length thus the inertia moment is $h^3/12$.

For an elastic response, the maximum stress (in the surface of the beam) must be smaller than the steel yield strength:

$$\sigma_m = \frac{M_{\max}}{\frac{h^3}{12}} \frac{h}{2} = \frac{\frac{4P_0 l^2}{8}}{\frac{h^3}{12}} \frac{h}{2} \le \sigma_y \tag{39}$$

which requires:

$$\frac{l}{h} \le \sqrt{\frac{\sigma_y}{3P_0}} \tag{40}$$

Given the steel yield strength σ_y as 500 MPa, with the peak free-field pressure, the relationship between beam span l and thickness h can be determined. Through calculation, the mild steel plate is chosen as 20 cm by 20 cm (effective span between two channel beam supports) with a thickness of 3.2 mm. And the standoff distances between the charge center and plate are chosen as 40 cm and 60 cm, respectively. It is worth noting that, to ensure the plate to deform elastically throughout the test, the above design for determining the plate dimension is conservative.

With the designed 3.2 mm thickness and standoff distance of 40 cm, the actual dynamic response factor of the test is calculated. The fundamental natural circular frequency of the beam representing the steel plate in the test is:

$$\omega = \sqrt{\frac{EI}{\rho A}}\left(\frac{\pi}{l}\right)^2 \tag{41}$$

It is worth noting that the Young's modus of the idealized beam is modified as $E/(1-\nu^2)$. With these parameters, the fundamental circular natural frequency is calculated as 1240 rad/s. Subsequently, the fundamental natural period of the beam is 5.1 ms.

The blast duration is twice the wave travel period from the detonation to the structure (TM5-855-1). Thus with the standoff distance 40 cm and wave velocity in the test site of 200 m/s, the blast duration is 4 ms.

From Fig. 6, the actual maximum response factor is around 1.5, which is over-estimated in design, allowing safety margin to ensure the structural member to remain elastic throughout the test.

The parameters for the test are:

The detailed parameters of the test are:

ρ=7800 kg/m^3 (density of mild steel)

E=210 GPa (Young's modulus of mild steel)

v=0.3 (Poisson's ratio of mild steel)

σ_y=500 MPa (yield strength of mild steel)

l=0.2 m (distance between the two channel beam supports)

h=0.0032 m (thickness of the plate, 3.2 mm)

c_s=200 m/s (acoustic velocity of wet fine sand)

n=3 (attenuation coefficient of wet fine sand)

f=1 (coupling factor for all tests, calculated from burial depth of charge 40 cm and the charge weight)

α (40 cm standoff distance)=0.8 (reduction factor)

α (60 cm standoff distance)=0.9 (reduction factor)

λ=0.1 (ratio of rise time to blast duration)

T_d (40 cm standoff distance)=4 ms (blast duration)

T_d (60 cm standoff distance)=6 ms (blast duration)

W=0.0105 kg (the charge for all tests is 10 g C-4, equivalent to 10.5 g TNT)

$\frac{R}{W^{1/3}}\left(40\,\text{cm standoff distance}\right)=1.8267\ m/kg^{1/3}$ (scaled distance)

$\frac{R}{W^{1/3}}\left(60\,\text{cm standoff distance}\right)=2.5752\ m/kg^{1/3}$ (scaled distance)

The acceleration time histories and strain at the plate center are recorded to validate the theoretical prediction.

5. Results and discussions

To compare with the test results, a case study with theoretical formulation is conducted. The tests are carried out twice for standoff distance 60 cm and once for standoff distance 40 cm. The acoustic velocity of the sand in the test site is 200 m/s, regardless of saturation degree. According to TM5-855-1, the blast duration is 6 ms for 60 cm standoff and 4 ms for 40 cm standoff. In addition, the attenuation coefficient for fine sand is adopted as 3, typical for sand [1]. Soil density is measured before each test. For the 60 cm standoff case, the soil density is taken as the average of the two tests, 1582 kg/m^3 while for the 40 cm standoff case, it is 1668 kg/m^3. Substituting these parameters into the theoretical analysis (for details, please refer to the appendix) leads to the predicted time histories of displacement, velocity and acceleration, as shown in Fig. 7.

Among the responses of the structural member, the acceleration time histories are most important, since they are the excitations to the attached secondary systems, i.e., the equipment within the main structure. From Fig. 7(c), the accelerations only oscillate once, which implies that the system consisting of the structural member and the surrounding soil is dominantly over-damped.

It is worth noting that the theoretical prediction in the present study is valid until the displacement achieves its peak. Before the peak displacement is achieved, the effect of surrounding soil on the structural member is applying ground shock (dynamic, particle velocity related pressure) in the same direction as the member moves, where the soil stiffness is not a concern (although soil stiffness is present in the empirical formula for peak free field pressure). When the structural member achieves peak displacement, it will bounce back. Then

the effect of the surrounding soil on the member is not only applying ground shock (dynamic, particle velocity related pressure), but also providing resistance due to its stiffness (static, not related to particle velocity). Therefore in the governing equation, in addition to the existing terms, an additional term representing the static stiffness effect of surrounding soil should be added. Subsequently, with different governing equation, the structural response will be different and the current prediction will be no longer valid. Then only the response time histories in the meaningful duration are presented.

To validate the predictions, the acceleration time histories obtained from the theoretical analysis and the small-scale test are compared, shown in Fig. 8. The peak values of predicted acceleration for 40 cm and 60 cm standoff are 250 g and 56 g, respectively. The predictions reasonably agree with the measurements, although not exactly the same. The predicted peak accelerations are higher than those of the tests, for both the cases of 40 cm and 60 cm standoff distance.

Recall that the rigid body motion of the whole test systems subjected to the soil-transmitted blast load is not considered in the model. In fact, the rigid body motion does exist in the test although its influence is insignificant due to the small ratio of the front plate mass to that of the whole set-up.

Differences between the predictions and test results do exist. First, the arrival time of the ground shocks are slightly different. The reason accounting for the difference in the arrival time is that in the theoretical prediction, a plane wave assumption is adopted. However, in the test, although compared to the plate dimension (20 cm by 20 cm), the standoff distance of 40 cm or 60 cm is relatively distant, the curvature of the blast does have some effects.

Subsequently the real arrival time is different: the mid-span of the plate is firstly loaded then the loading area increases with time from the mid-span towards the supports. On the contrary, in the theoretical prediction, the plane wave is applied to the whole plate uniformly at the same time when the wave hits the mid-span of the plate. Therefore the major peaks of the tested acceleration time histories are relatively later compared to those predicted.

Second, the positive parts of the acceleration time history are over-predicted while the negative parts are under-predicted. The reason is still the plane wave assumption. Take the over-predicted positive peak as example. In the real situation, at first the mid-span part is loaded first while other parts are not loaded, resulting in relatively gentle acceleration rise at the beginning. In a short while, the loading in the mid-span decreases quickly and the other parts are loaded. However, these details cannot be captured by a plane wave model, which leads to sharper rise at the beginning and higher peaks.

In addition, the trends of the predicted acceleration time histories are similar to those of the tests: they do not oscillate, implying the plate is over-damped by the presence of the surrounding soil, which is favorably predicted by the model.

To further verify the theoretical model, the tested strain time history at the plate center is also compared to that of the prediction. It is evident that the strain time history at the beam mid-span has the same trend as that of the displacement. From simple calculation based on the strength of materials, they are linked as follows:

$$\varepsilon = \frac{24wh}{5l^2} \tag{42}$$

where ε and w are the strain and displacement at the mid-span, respectively. l is the span and h is the thickness of the structural member. From Eq. (42), the strain time history in fact is the

displacement time history multiplied by a constant. Figure 9 indicates that the trend and peak value of the predicted strain time history compare favorably with those of the test.

Based on the verification and validation of the acceleration and strain time histories, the model in the present study reasonably predicts the responses of an underground structural member subjected to a ground shock.

Further, this validated model is used as a benchmark to evaluate the accuracy of the model without considering the ground shock rise time [12]. With the same parameters, two models with and without considering the rise time, are compared in Fig. 10. It can be seen that the differences of displacement and velocity time histories at mid-span are not significant. The displacement for ground shock with zero rise time is higher in the initial stage and achieves its peak slightly earlier. Similarly, the velocity for ground shock with zero rise time also achieves peak earlier. Even though, the peak displacements and velocities of the two models are nearly the same no matter the ground shock rise time is considered or not.

However, from Fig. 10(c), the profiles of the acceleration time histories at mid-span are significantly different. Subjected to ground shock with zero rise time, the acceleration achieves its peak at time zero and decreases with time rapidly; in contrast, when the rise time is taken into account, the acceleration is zero initially and has a profile with a substantially lower peak and a longer duration. This significant discrepancy will lead to different vibration characteristics of the attached secondary system thus should be carefully examined when designing underground facilities.

In fact, the acceleration time histories in Fig. 10(c) are the excitations to the attached equipment and devices. To evaluate the shock level experienced by a specific device, shock

response spectra with the acceleration time history of the main structure as input [22] are established, shown in Fig. 11. It is interesting that intuitively the ground shock with zero rise time results in an acceleration time history with a significantly high peak as the excitation, which may subsequently lead to a severer shock level to the contained equipment. However, in the present case study, the maximum acceleration on the device by ground shock with non-zero rise time is higher, which is not as expected. In fact, Fig. 10(c) reveals the underlying mechanism: when subjected to a ground shock with zero rise time, the acceleration peak is significantly higher, but the shock duration is shorter. In contrast, when subjected to ground shock with non-zero rise time, the acceleration excitation peak is relatively lower, but the duration is longer. The difference in the shock duration significantly influences the responses of the attached equipment: the device with support of higher natural frequency should be effectively excited by the shock with zero rise time while the responses induced by non-zero rise time should be higher for device with support of relatively lower natural frequency. According to the trends of the curves, these two curves may intersect at certain frequency higher than 1000 Hz, after which the shock level of ground shock with zero rise time is higher. However, in a practical range of devices with support, i.e. 1 Hz to 1000 Hz, the shock level on equipment is higher for ground shock with non-zero rise time.

6. Conclusions

In-structure shock of underground structures is theoretically investigated with ground shock rise time taken into consideration. A small scale test is designed and conducted to validate the analytical prediction. When the scaled model of an underground structure is installed in wet

fine sand and subjected to a ground shock induced by a small scale subsurface detonation, the acceleration time histories favorably compare with the theory. The predicted peak accelerations are slightly higher than those of the tests and the profiles are in reasonable agreement with the test. Further verification of the model is made by comparing the predicted and tested strain time histories at the plate center. With the current model considering ground shock rise time as a benchmark, the model with zero rise time is discussed. It is found that, with and without considering the rise time, the displacements and velocities are similar but the acceleration time histories are significantly different. In the practical range of devices with support, i.e. 1 Hz to 1000 Hz, the shock level on equipment by ground shock with non-zero rise time is higher. The prediction can be used as a supplement to the design codes. It is recommended that in preliminary design of underground structures, the rise time of ground shock should be considered when assessing in-structure shock.

Acknowledgement

The corresponding author would like to acknowledge the support of the Collaborative Research Fund with Overseas, Hong Kong and Macau Scholars (Grant number 51028801) of the National Natural Science Foundation of China.

References

[1] US Army Engineers Waterways Experimental Station. Fundamentals of protective design for conventional weapons, TM5-855-1. Vicksburg; 1986.

[2] Dancygier AN, Karinski YS. A simple model to assess the effect of soil shear resistance on the response of soil buried structures under dynamic loads. Eng Struct 1999;21: 1055-65.

[3] Dancygier AN, Karinski YS. Response of a buried structure to surface repetitive loading. Eng Struct 1999;21: 416-24.

[4] Stevens DJ, Krauthammer T. A finite difference/finite element approach to dynamic soil-structure interaction modeling. Comput Struct 1988;29 (2): 199-205.

[5] Chen Y, Krauthammer T. A combined Adina-finite difference approach with substructure for solving seismically induced nonlinear soil-structure interaction problems. Comput Struct 1989;32 (3-4): 779-85.

[6] Stamos AA, Beskos DE. Dynamic analysis of large 3-D underground structure by the BEM. Earthquake Eng Struct Dynamics 1992;24: 917-34.

[7] Ma GW, Hao H, Zhou YX. Assessment of structure damage to blasting induced ground motions. Eng Struct 2000;22: 1378-89.

[8] Sackman JL, Kelly JM. Seismic analysis of internal equipment and components in structures. Eng Struct 1979; 1: 179-90.

[9] Hernried AG, Jeng H. Dynamic response of secondary systems in structures subjected to ground shock or impact. Eng Struct 1987; 9: 19-26.

[10] Hernried AG, Lau KS. Dynamic response of tertiary systems in structures subjected to base excitation. Eng Struct 1988; 10: 185-93.

[11] Alwis WAM, Lam KY. Response spectrum of underground protective structures. Finite Elem Anal Des 1994;18: 203-09.

[12] Ma GW, Zhou HY, Lu Y, Chong K, In-structure shock of underground structures: a theoretical approach. Eng Struct 2010; 32: 3836-44.

[13] Ma GW, Zhou HY, Chong K. In-structure shock assessment of underground structures with consideration of rigid body motion. J Eng Mech-ASCE 2011;137(12): 797-806.

[14] Zhou HY, Ma GW. Double-layer floor to mitigate in-structure shock of underground structures: a conceptual design. Eng Struct 2012;35: 314-21.

[15] Wong FS, Weidlinger P. Design of underground protective structures. J Struct Eng-ASCE, 1983;109 (8): 1972-79.

[16] Weidlinger P, Hinman E. Analysis of underground protective structures. J Struct Eng-ASCE 1988;114 (7): 1658-73.

[17] Melosh HJ. Shock viscosity and rise time of explosion waves in geologic media. J Appl Phys 2003; 94(7): 4320-25.

[18] Anand S. Measurement and modeling of ground response due to dynamic loading. Ph.D. thesis. Singapore: Nanyang Technological University; 2007.

[19] Biggs JM. Introduction to structural dynamics. New York: McGraw-Hill; 1964.

[20] Clough RW, Penzien J. Dynamics of structures. New York: McGraw-Hill; 1993.

[21] Smith PD, Hetherington JG. Blast and ballistic loading of structures, Butterworth-Heinemann, London, 1994.

[22] Gupta AK. Response spectrum method in seismic analysis and design of structures. Boca Raton: CRC press; 1992.

[23] Beppu M, Okagaki K, Katayama M, Itoh M. Numerical simulation on soil pressure due to underground explosion. Eurodyn 2011: 8th International Conference on Structural Dynamics, July 4-6, 2011, Leuven, Belgium.

[24] Gere JM, Mechanics of Materials, 6th edition, Cengage Learning, 2004.

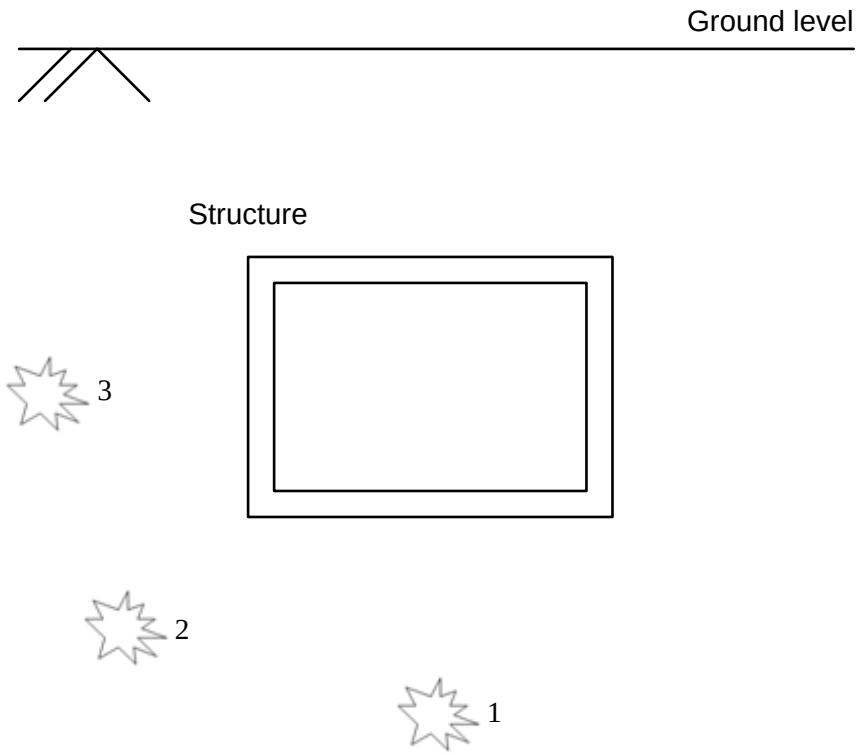

Fig. 1 An underground structure subjected to subsurface detonations of various locations

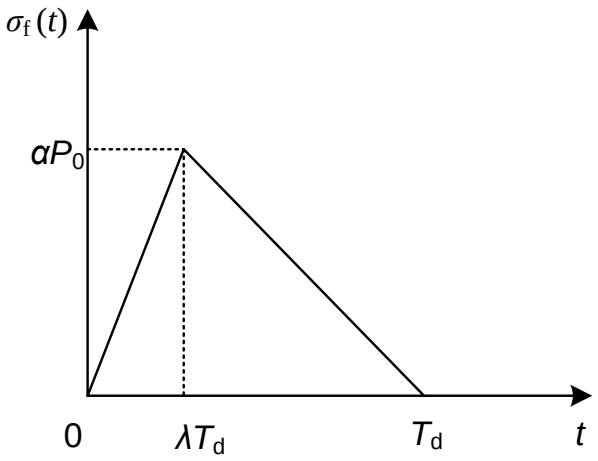

Fig. 2 The idealized profile of a free field ground shock

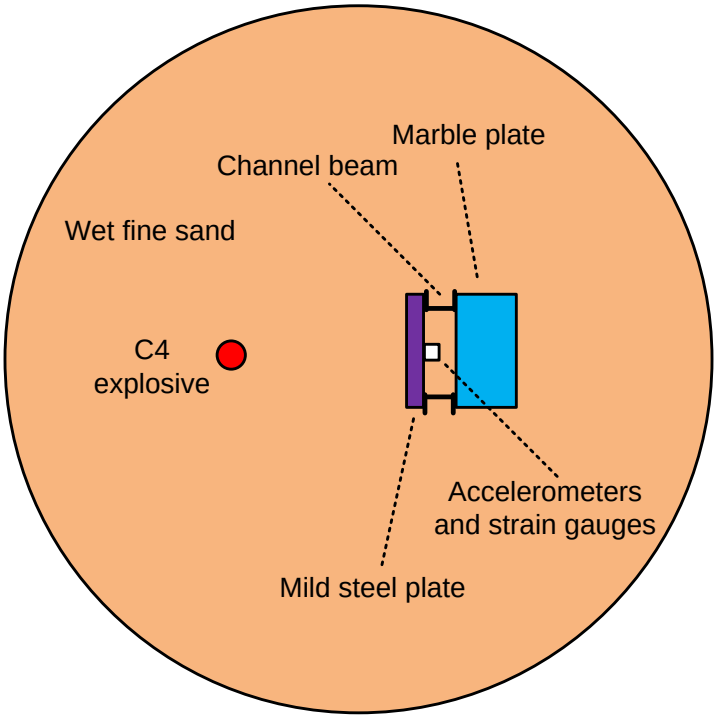

(a)

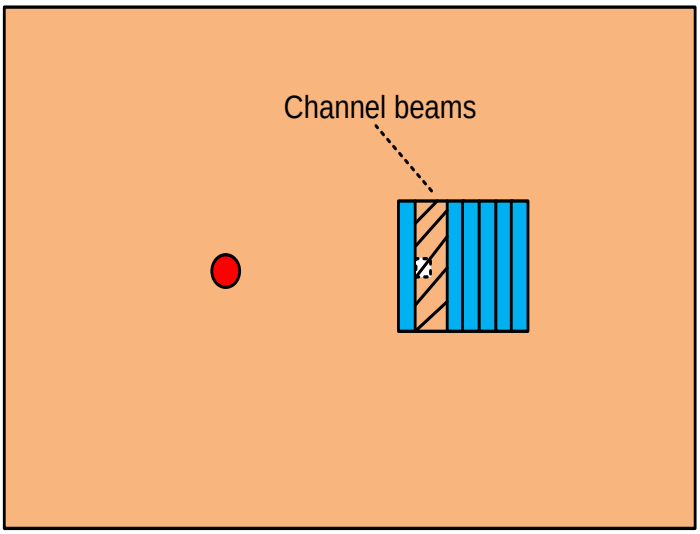

(b)

Fig. 3 The designed test set-up (not to scale): (a) plan view; (b) side view

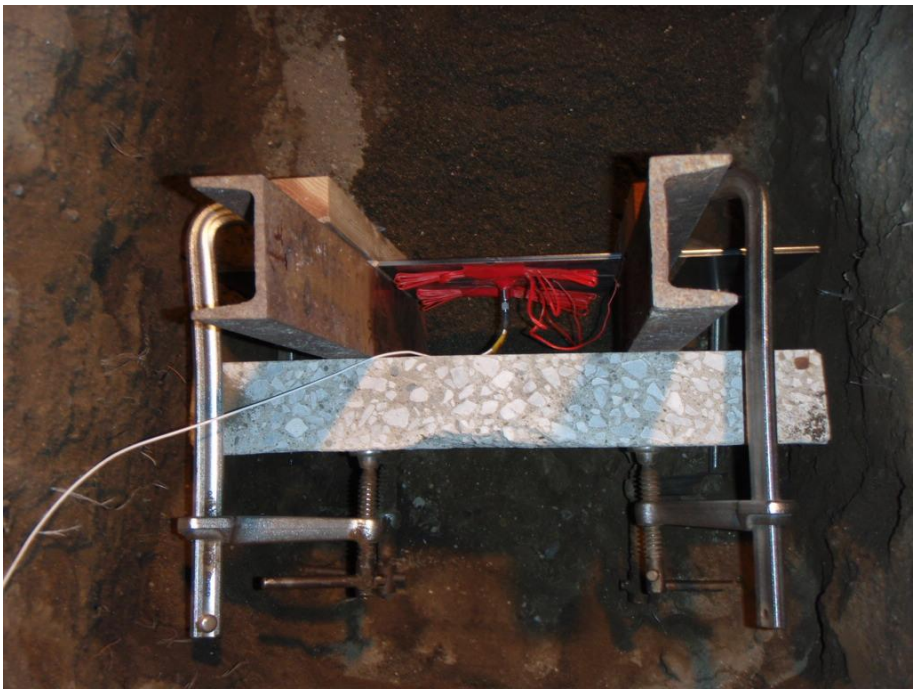

(a)

(b)

Fig. 4 The small scale test set-up

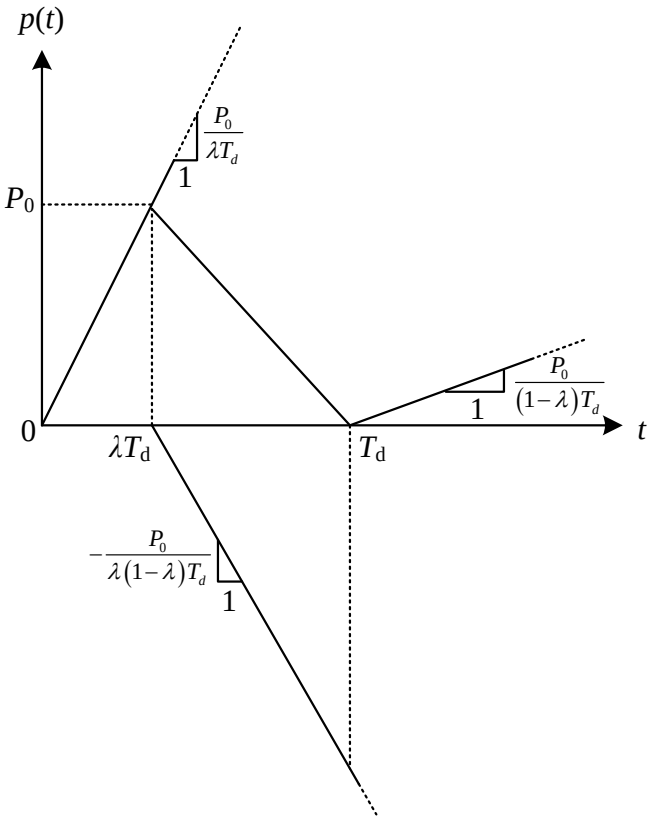

Fig. 5 Ground shock with non-zero rise time is considered as superposition of three ramp loadings with different starting time

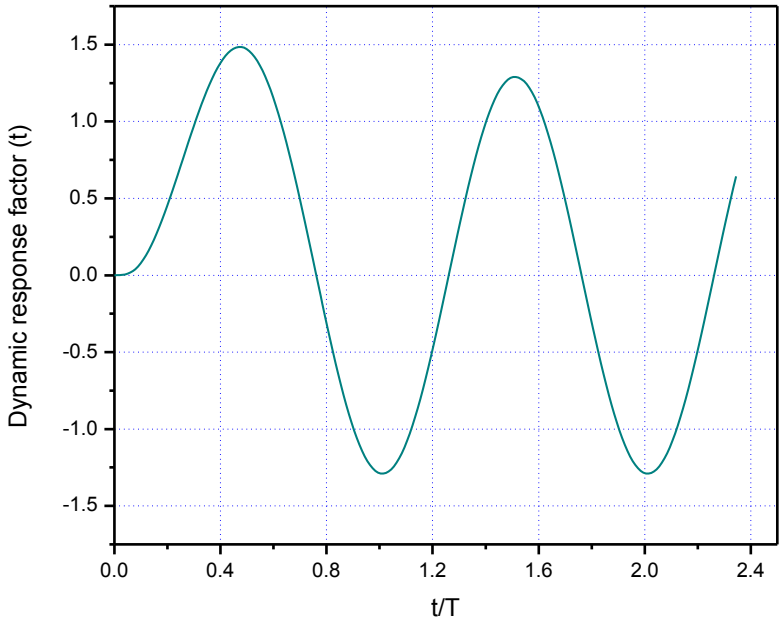

Fig. 6 Dynamic response factor of triangular load (λ=0.1). *t* is time and *T* is natural period of structure

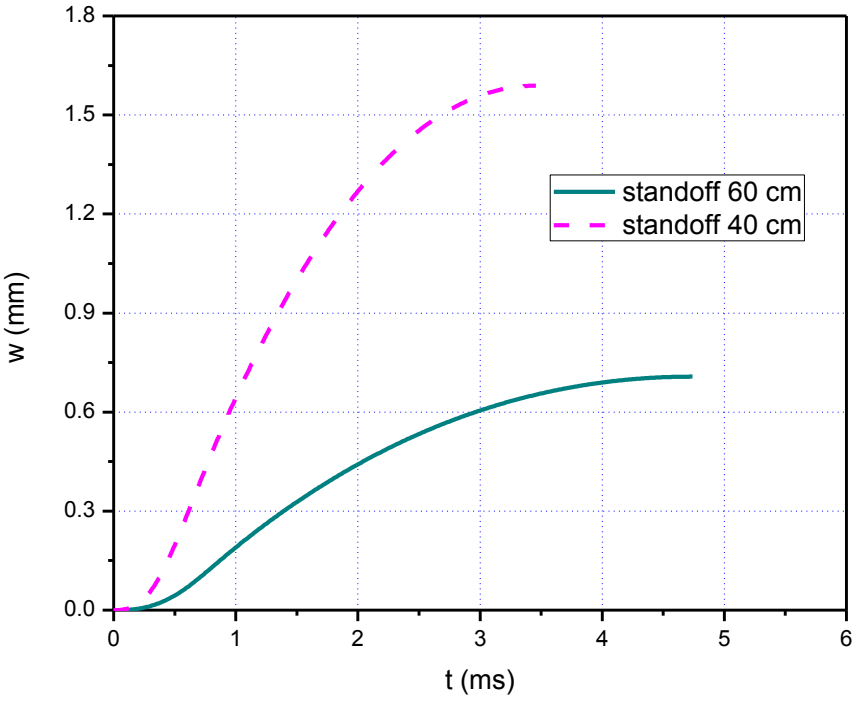
w (mm)
t (ms)
standoff 60 cm
standoff 40 cm
0.0
0.3
0.6
0.9
1.2
1.5
1.8
0
1
2
3
4
5
6

(a)

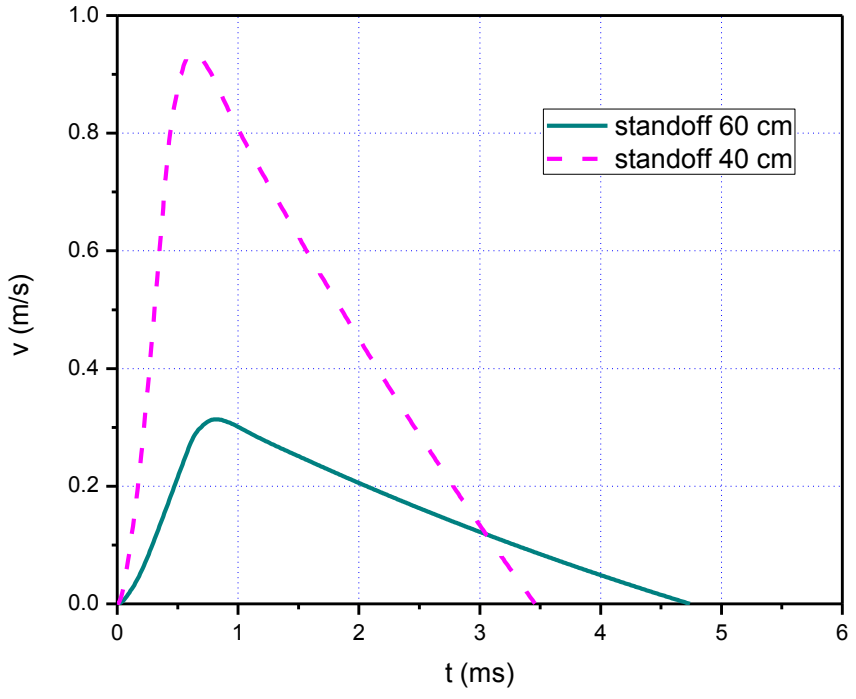
v (m/s)
t (ms)
standoff 60 cm
standoff 40 cm
0.0
0.2
0.4
0.6
0.8
1.0
0
1
2
3
4
5
6

(b)

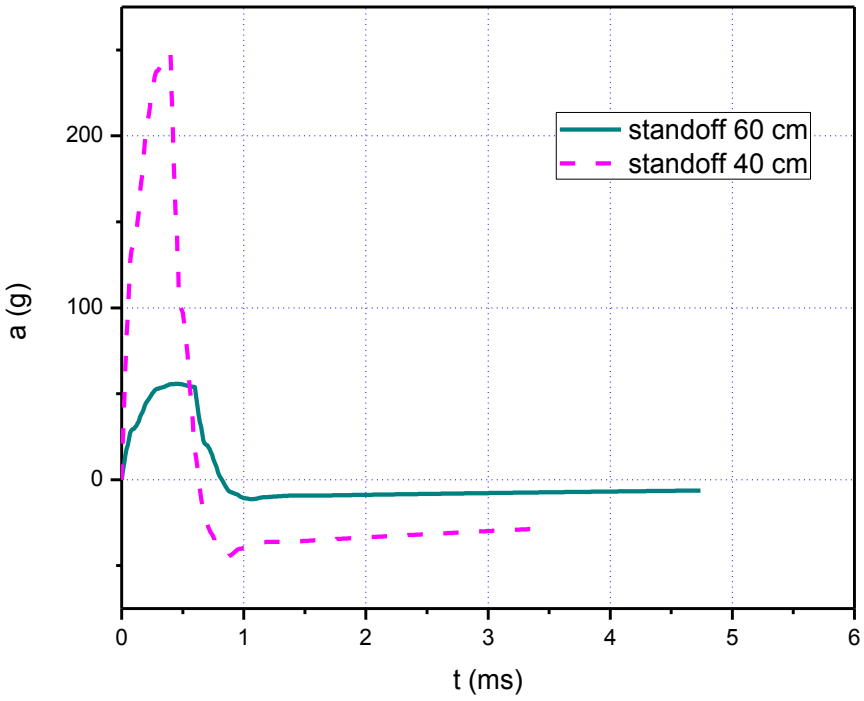

(c)

Fig. 7 Predicted response time histories at mid-span of structural member: (a) displacement; (b) velocity; (c) acceleration

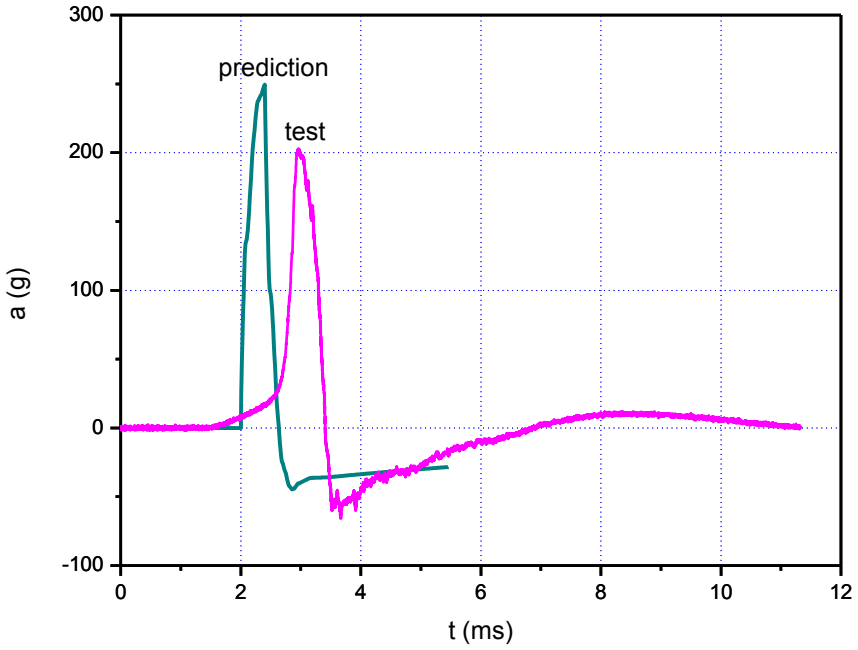

(a)

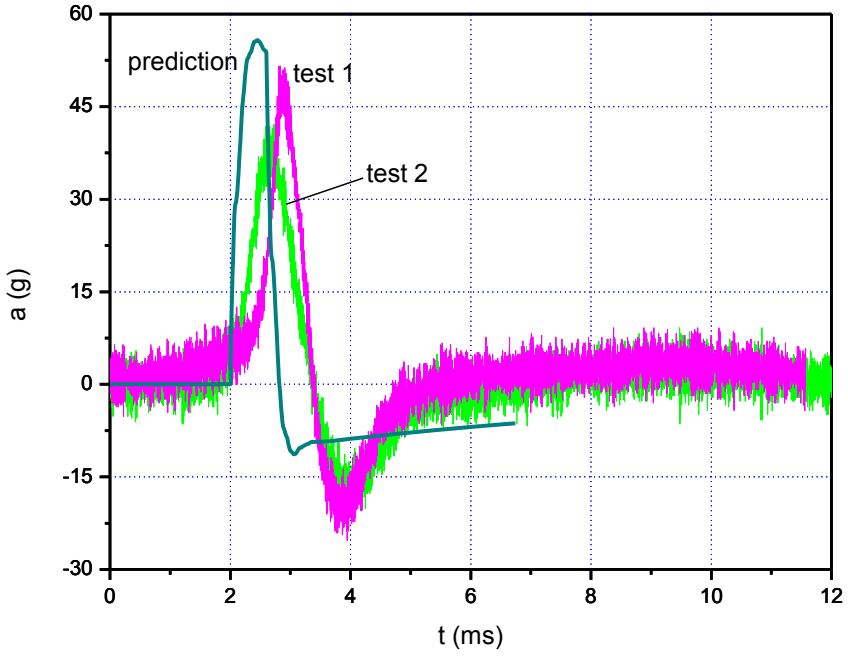

(b)

Fig. 8 Comparison of the predicted and tested acceleration time histories: (a) 40 cm standoff distance; (b) 60 cm standoff distance

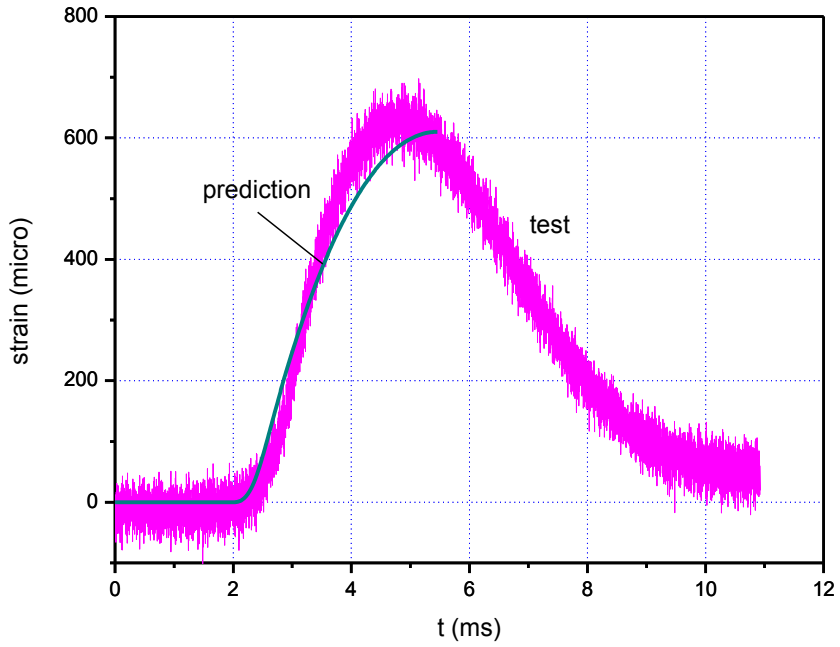

Fig. 9 Comparison of the predicted and tested strain time history at the plate center: 40 cm standoff distance

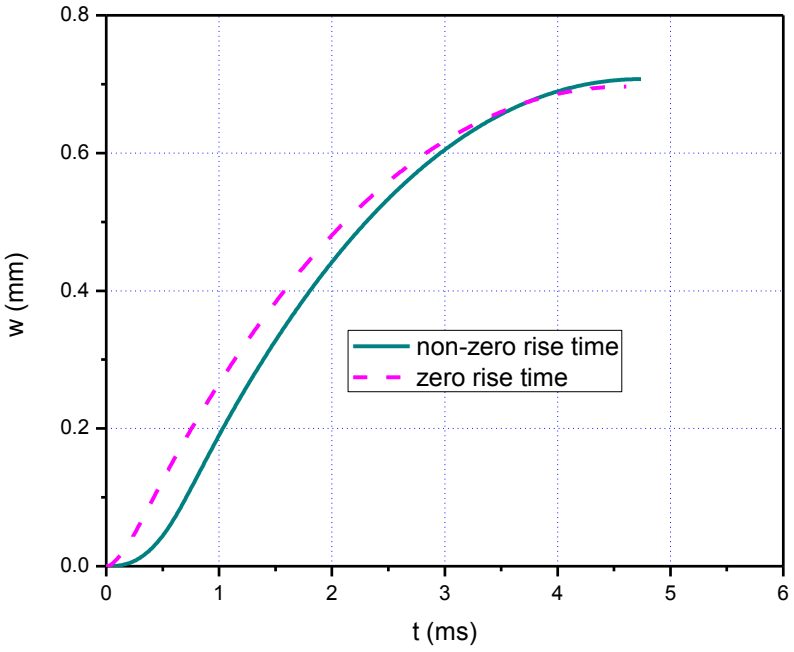
0.8
0.6
0.4
0.2
0.0
w (mm)
0
1
2
3
4
5
6
t (ms)
non-zero rise time
zero rise time

(a)

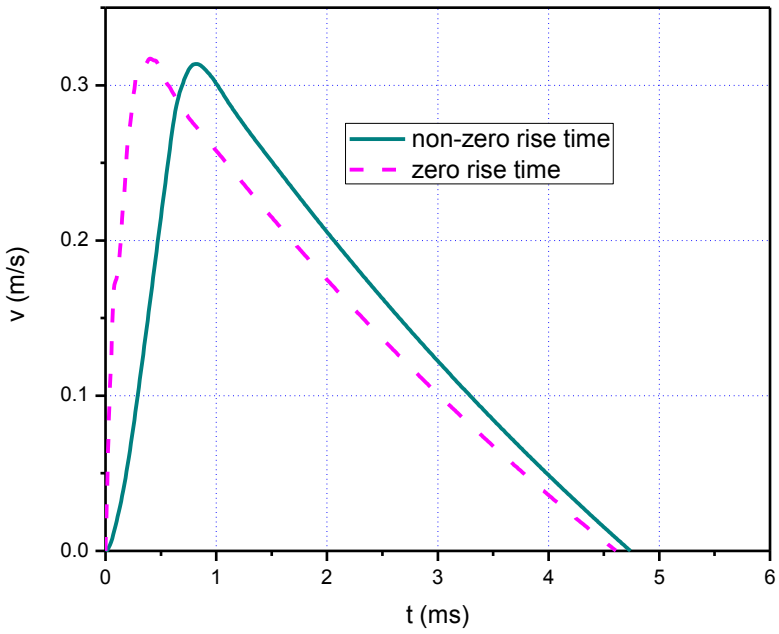
0.3
0.2
0.1
0.0
v (m/s)
0
1
2
3
4
5
6
t (ms)
non-zero rise time
zero rise time

(b)

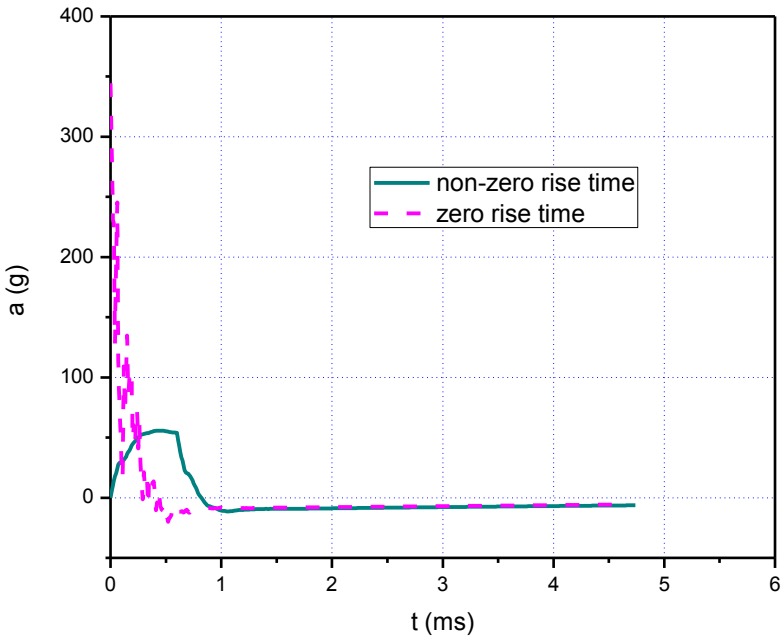

(c)

Fig. 10 Comparison of the structural response with and without ground shock rise time: 60 cm standoff distance

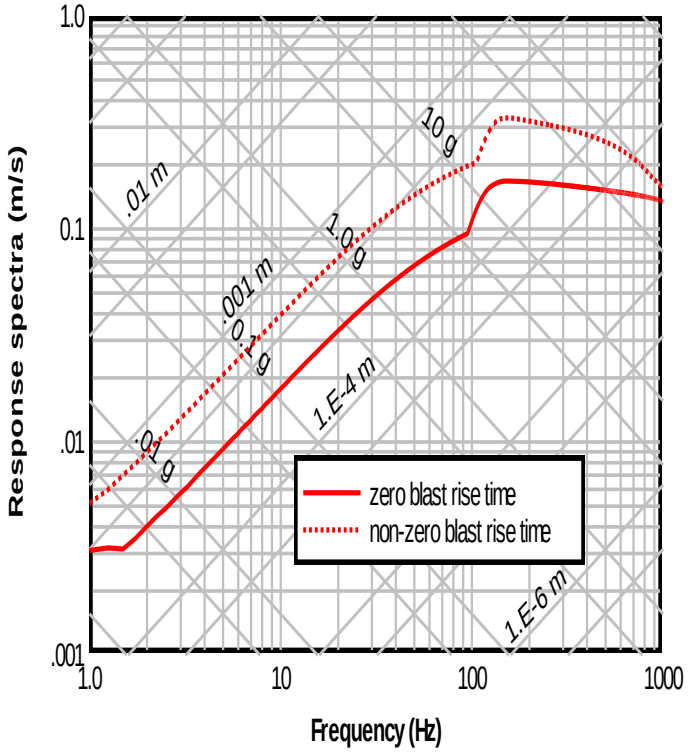

Fig. 11 Response spectra comparison of ground shocks with zero and non-zero rise time: 60 cm standoff distance